Bistatic Model of Ocean Scattering

Giovanni Picardi, Roberto Seu, Stefano G. Sorge, and Manuel Martin Neira

***Abstract*—An analytical closed-form model is derived for the average power echo received by a bistatic altimeter from an oceanic surface at a frequency high enough for the Kirchhoff scattering mechanism to be dominant over the Bragg resonance one. The asymmetric behavior of the sea waves is taken into account, modeling the surface height as a non-Gaussian distributed random process and an explicit expression of the so-called "electromagnetic bias" is obtained as a function of the skewness coefficient of the distribution. Results obtained applying such model to a monostatic geometry are shown to be in good agreement with those reported in literature as well as with those obtained by numerical simulations. It is also shown that, letting the "non-Gaussianity" term tend to zero, our model correctly reduces to the well-known Brown model for Gaussian surfaces. This work has been conceived in the frame of the feasibility study of a bistatic remote sensing system, consisting of a constellation of satellites flying at the same altitude with an operating geometry such that the incidence and scattering angles are equal.**

***Index Terms*—Sea surface electromagnetic scattering.**

I. Introduction

MONOSTATIC radar altimeter returns from ocean have been well studied and models have been developed [1] that describe the echo waveform characteristics. What has not been so well investigated is the operation of a bistatic radar altimeter measuring the ocean surface, which could have some relevance in future earth remote sensing systems, in particular for sensors operating in the Ku-band [2].

A bistatic radar system presents some differences with respect to a monostatic one [3]. The constant range loci are ellipsoids whose foci are located at the transmitter and receiver; these ellipsoids intersect the ground, forming ellipses so that spatial resolution is achieved over elliptical areas. Furthermore, these ellipses are, in general, tilted with respect to the iso-Doppler lines as these depend on the relative direction of motion of both transmitter and receiver. Finally, the iso-power lines form the so-called ovals of Cassini, quite different from the circles we find in the monostatic case.

As a consequence, the bistatic return waveform from the ocean looks different as compared to the monostatic one. This paper shows these differences by providing an extension of the Brown model to a bistatic geometry and a non-Gaussian surface. Such bistatic model will be useful to study the feasibility of a bistatic altimeter and to evaluate the performance of such a system in the estimate of the distance from a reference average surface, of the surface roughness and of the surface backscattering coefficient. In particular, the model is intended for the assessment of the performance of a constellation of satellites flying at the same altitude (say 800 km) and with an operating geometry such that the incidence and scattering angles are equal. This kind of geometry can be shown to be the most meaningful for a bistatic system; in fact, it has been demonstrated in [2] that the point of specular reflection is the center of symmetry of the isorange lines and it is also the point on the surface with the minimum bistatic radar path. The model has been worked out applying the Kirchhoff approximation to a gently undulating (small rms slope) rough surface and considering that the geometric optics mechanism dominates the Bragg scattering mechanism [6].

II. Scattering from an Irregular Flat Surface Illuminated by a Radar Pulse

It is well known that if the transmitting antenna of a monochromatic continuous wave bistatic radar illuminates an irregular flat surface, the scattered electric field E_S at the receiver antenna can be evaluated under the Kirchhoff approximation[1] as discussed in [4] (see also Fig. 1)

$$E_S = -\frac{j}{2\lambda}\int_S G(P)\cdot R(P)\cdot \frac{\hat{n}\cdot(\hat{R}_1-\hat{R}_3)}{R_1R_3} \cdot e^{-jk(R_1+R_3)}\,dS \tag{1}$$

where $E_i = (1/R_1)e^{-jkR_1}$ is the incident spherical wave, λ is the wavelength, $G(P)$ is the antenna gain in the direction of a generic point P on the surface S, $R(P)$ is the Fresnel reflection coefficient, R_1 and R_3 are, respectively, the distances from transmitter to the point P and from the point P to the receiver, $\hat{R}_{1(3)}$ is the unit vector corresponding to the path from the transmitter (receiver) to the point P, $\hat{n}$ is the unit vector normal to the surface in the point P, and finally $k = 2\pi/\lambda$ is the wave number.

If, on the contrary, the radar transmits a pulse $f(t)$, thanks to the superimposition principle for linear media, the scattered

Manuscript received July 24, 1997; revised April 6, 1998. This work was supported by a Research Contract of Alenia Spazio in the frame of a mission study sponsored by the European Space Agency (ESA).

G. Picardi, R. Seu, and S. Sorge are with the INFOCOM Department, University of Rome La Sapienza, Rome, Italy, S.T.S. Studi, Tecnologie e Sistemi Srl, Rome, Italy.

M. M. Neira is with ESA-ESTEC, Noordwijk, The Netherlands.

Publisher Item Identifier S 0018-926X(98)07502-4.

[1]It should be noticed that (1) does not account for the effects of the depolarized scattering component. This effect could be taken into account by means of a matrix approach to include shadowing and multiple scattering effects in the evaluation of the bistatic scattering coefficient as discussed in [17]. Anyway, in our case such component is usually negligible due to the relatively small surface root mean square (rms) slopes (<0.4) and incidence angles (typically less than 45°).

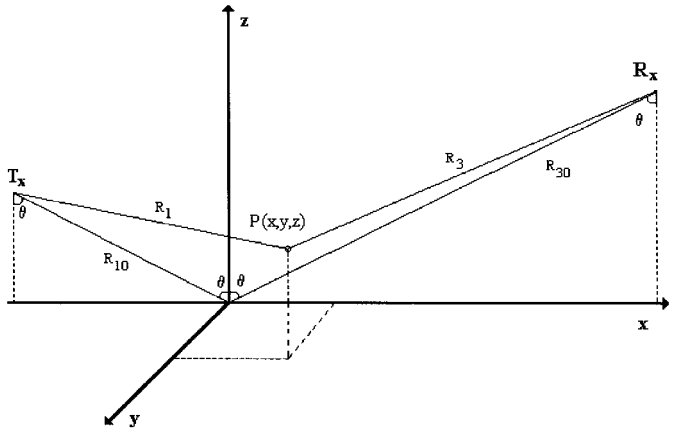

Fig. 1. Geometry for the evaluation of the bistatic scattering: Tx is the transmitter location, Rx is the receiver location.

electric field becomes

$$E_S(t) = \int_{-\infty}^{\infty} F(\omega) \cdot \left(-\frac{j}{2\lambda}\right) \int_S G(P) \cdot R(P) \cdot \frac{\hat{n} \cdot (\hat{R}_1 - \hat{R}_3)}{R_1 R_3} \cdot e^{-jk(R_1+R_3)}\, dS\, e^{j\omega t}\, d\omega \quad (2)$$

where $F(\omega)$ is the Fourier transform of the transmitted pulse.

Without affecting the generality of the results we can assume a rectangular antenna pattern within the beam width $G(P) = 1$. Moreover, since Kirchhoff surfaces are such that the local radius of curvature of the surface is larger than the incidence wavelength, we can confuse the local normal to the generic surface element with the vertical axis $\hat{n} \approx \hat{z}$. Further assuming that the local incidence angle slightly varies around the specular reflection angle, we can write $\hat{n} \cdot (\hat{R}_1 - \hat{R}_3) = 2 \cos \theta$. The above simplifications hold for a small root mean square (rms) slope surface and a narrow antenna beam width (see also [4]).

Finally, under the Fresnel hypothesis, an approximated expression for the distances R_1 and R_3 can be used (see Fig. 1)

$$\begin{aligned} R_1 &\approx R_{10} + x \sin\theta - z \cos\theta + \frac{x^2+y^2}{2R_{10}} \\ R_3 &\approx R_{30} - x \sin\theta - z \cos\theta + \frac{x^2+y^2}{2R_{30}} \end{aligned} \quad (3)$$

where the meaning of the symbols R_{10}, R_{30}, and θ is clear from Fig. 1 and z (the surface height) is, by definition, a zero mean random variable. Summing up R_1 and R_3, we have

$$R_1 + R_3 \approx R_{10} + R_{30} - 2z \cos\theta + \frac{x^2+y^2}{2R_p} \quad (4)$$

where

$$R_p = \frac{R_{10} R_{30}}{R_{10} + R_{30}}.$$

The errors due to the above approximations will be checked on the derived model by comparison with direct numerical simulations of the integral in (1). Substituting (3) and (4) in (2) the power associated to the scattered electric field can be directly evaluated

$$\begin{aligned} &\langle E_S(\tau) \cdot E_S^*(\tau) \rangle \\ &= \frac{4\Gamma(\theta)}{(4\pi c R_{10} R_{30})^2} \cos^2\theta \int d\omega_1 \cdot \int d\omega_2 \omega_1 \omega_2 F(\omega_1) \\ &\quad \cdot F^*(\omega_2) e^{j(\omega_1 - \omega_2)\tau} \int_{S_1} dS_1 \int_{S_2} dS_2 \\ &\quad \cdot \exp\left(-\frac{j}{2R_p c}\left[\omega_1(x_1^2 + y_1^2) - \omega_2(x_2^2 + y_2^2)\right]\right) \\ &\quad \cdot \left\langle \exp\left(j \frac{2\cos\theta}{c}(\omega_1 z_1 - \omega_2 z_2)\right)\right\rangle \end{aligned} \quad (5)$$

where $\Gamma(\theta) = |R(P)|^2$ is the surface Fresnel reflectivity, $\tau = t - (R_{10} + R_{30})/c$ and

$$\begin{aligned} &\left\langle \exp\left(j \frac{2\cos\theta}{c}(\omega_1 z_1 - \omega_2 z_2)\right)\right\rangle \\ &= \int\int p(z_1, z_2) \cdot \exp\left(j \frac{2\cos\theta}{c}(\omega_1 z_1 - \omega_2 z_2)\right) \\ &\quad \cdot dz_1 \cdot dz_2 \end{aligned} \quad (6)$$

is the joint characteristic function of the random variables z_1 and z_2, say $\phi(z_1, z_2)$ [8], [9], [11], computed at $z_1 = ja\omega_1$, $z_2 = -ja\omega_2$ with $a = (2\cos\theta)/c$. Such characteristic function can be expressed as a power series

$$\phi(z_1, z_2) = \sum_{i,r} \frac{m_{ir}}{i!r!} \cdot z_1^i z_2^r \quad (7)$$

being the m_{ir} coefficients the moments of the distribution $m_{ir} = \langle z_1^i z_2^r \rangle$. The cumulants of the distribution k_{ij} are defined as the coefficients of the analogous expansion of the function

$$\log \phi(z_1, z_2) = \sum_{i,r} \frac{k_{ir}}{i!r!} \cdot z_1^i z_2^r \quad (8)$$

and can be computed by the following relation obtained inverting the Mc-Laurin series

$$k_{ir} = \frac{\partial^{i+r}}{\partial z_1^i\, \partial z_2^r} \log \phi \Big|_{z_1 = z_2 = 0}. \quad (9)$$

From the above equation, it is clear that the cumulants k_{ir} will be polynomial combination of the moments m_{ir}

$$\begin{aligned} k_{10} &= m_{10} \\ k_{20} &= m_{20} - m_{10}^2 \\ k_{30} &= m_{30} - 3m_{10}m_{20} + 2m_{10}^3 \\ k_{21} &= m_{21} - m_{20}m_{01} - 2m_{10}m_{11} + 2m_{10}^2 m_{01} \\ &\cdots \\ k_{01} &= m_{01} \\ k_{02} &= m_{02} - m_{01}^2 \\ k_{03} &= m_{03} - 3m_{01}m_{02} + 2m_{01}^3 \\ k_{12} &= m_{12} - m_{02}m_{10} - 2m_{01}m_{11} + 2m_{01}^2 m_{10} \\ k_{11} &= m_{11} - m_{01}m_{10}. \end{aligned} \quad (10)$$

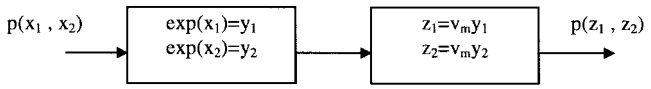

Fig. 2. Conceptual scheme for the evaluation of the non-Gaussian, two-dimensional surface–height distribution.

It is easy to verify that apart from the first-order cumulants k_{10} and k_{01}, the expression reported above correspond to the central moments of the distribution $\mu_{ir} = \langle (z_1 - m_{10})^i (z_2 - m_{01})^r \rangle$.

In order to solve the integral it is necessary to make some assumptions about the surface roughness. It is now well known that the ocean surface cannot be considered Gaussian, as suggested by Brown [1], on the evaluation of the average echo. As a matter of fact, due to the nonlinear interaction at the interface between the water and the air, the wave crests are more peaked than the wave troughs and this effect can be taken into account by giving to the surface height probability density function (pdf) a nonsymmetric behavior that is a nonzero skewness coefficient [7], [10], [11].

This has been done in our analysis applying an exponential nonlinearity to a bivariate Gaussian distribution $p(x_1, x_2)$ (see the scheme in Fig. 2) with mean value equal to zero, standard deviation σ_g and Gaussian correlation function ρ. In addition, a proper final gain v_m gives reason of the actual roughness value: a bivariate lognormal model $p(z_1, z_2)$ arises with parameters v_m (the median value), σ_g (the shape factor) and cross-correlation function proportional to ρ. In particular, for small values of σ_g, that is a condition fully compatible with our operating conditions, we can work out the following relationships [12]:

$$\mu_{20} = \mu_{02} \cong v_m^2 \sigma_g^2 = \sigma_h^2 \tag{11}$$

$$\mu_{11} \cong v_m^2 \sigma_g^2 \rho(r') = \sigma_h^2 \lambda_{11} \tag{12}$$

$$\mu_{12} = \mu_{21} \cong v_m^3 \sigma_g^4 \rho(r')[2 + \rho(r')] = \sigma_h^3 \lambda_{12} \tag{13}$$

$$\mu_{30} = \mu_{03} \cong v_m^3 \cdot 3\sigma_g^4 = \sigma_h^3 \lambda_3 \tag{14}$$

where λ_{ij} are the normalized moments of the bivariate lognormal distribution and $\lambda_3 \approx 3\sigma_g$ is the skewness coefficient. In [10], it is assessed that the maximum value of surface skewness obtained experimentally is about 0.3, that is the maximum value of the parameter σ_g is about 0.1 and in this case the error due to the approximations (11)–(14) is in the order of 10^{-4} in the worst case (μ_{20}, [12]).

Introducing (11)–(14) in (6), we can write

$$\left\langle \exp\left(j \frac{2\cos\theta}{c} (\omega_1 z_1 - \omega_2 z_2) \right) \right\rangle \cong \exp\left(-\tfrac{1}{2} a^2 \sigma_h^2 [\omega_1^2 - 2\lambda_{11}\omega_1\omega_2 + \omega_2^2]\right) \cdot \exp\left(-\frac{j}{6} a^3 \sigma_h^3 [\lambda_3 \omega_1^3 + 3\lambda_{12}\omega_1\omega_2^2 - 3\lambda_{21}\omega_1^2\omega_2 - \lambda_3 \omega_2^3] \right). \tag{15}$$

We can now make the approximation of small fractional bandwidth, that is

$$\omega_1^3 - \omega_2^3 \cong 3\omega_1\omega_2(\omega_1 - \omega_2) \tag{16}$$

obtaining

$$\left\langle \exp\left(j \frac{2\cos\theta}{c} (\omega_1 z_1 - \omega_2 z_2) \right) \right\rangle \cong \exp\left(-\frac{1}{2} a^2 \sigma_h^2 (\omega_1 - \omega_2)^2 \right) \cdot \exp\left(-a^2 \sigma_h^2 [1 - \rho(r')] \omega_1 \omega_2 \right) \cdot \exp\left(-\frac{j}{2} a^3 \sigma_h^3 \lambda_3 \omega_1 \omega_2 (\omega_1 - \omega_2) \cdot \left[1 - \tfrac{2}{3}\rho(r') - \tfrac{1}{3}\rho^2(r')\right] \right). \tag{17}$$

Considering a Gaussian model for the wave height correlation, and assuming a surface rough enough in order for the geometric optics mechanism to be dominant, the correlation function can be well represented by the only first-order term of its series expansion [6] yielding

$$\rho(r') = e^{-(r'^2/l^2)} \cong 1 - \frac{r'^2}{l^2}. \tag{18}$$

Introducing this expression in (17), we have

$$\left\langle \exp\left(j \frac{2\cos\theta}{c} (\omega_1 z_1 - \omega_2 z_2) \right) \right\rangle \cong \exp\left(-\frac{1}{2} a^2 \sigma_h^2 (\omega_1 - \omega_2)^2 \right) \exp\left(-a^2 \sigma_h^2 \frac{r'^2}{l^2} \omega_1 \omega_2 \right) \cdot \exp\left(-\frac{j2}{3} a^3 \sigma_h^3 \lambda_3 \omega_1 \omega_2 (\omega_1 - \omega_2) \frac{r'^2}{l^2} \right) \tag{19}$$

and the average power associated to the scattered electric field given by (5) can be rewritten as follows:

$$\langle E_s(\tau) E_s^*(\tau) \rangle = \frac{4\Gamma(\theta)\cos^2\theta}{(4\pi c R_{10} R_{30})^2} \cdot \int_{-\infty}^{+\infty} \int_{-\infty}^{+\infty} \omega_1 \omega_2 F(\omega_1) F^*(\omega_2) \cdot e^{j(\omega_1 - \omega_2)\tau} e^{-(1/2)a^2\sigma_h^2(\omega_1 - \omega_2)^2} I(\omega_1, \omega_2)\, d\omega_1\, d\omega_2 \tag{20}$$

where

$$I(\omega_1, \omega_2) = \int_{S_1} \int_{S_2} \exp\left(-j \frac{1}{2cR_p} [\omega_1 (x_1^2 + y_1^2) - \omega_2 (x_2^2 + y_2^2)] \right) \cdot \exp\left(-a^2 \sigma_h^2 \omega_1 \omega_2 \frac{r'^2}{l^2} \right) \cdot \exp\left(-j \frac{2}{3} a^3 \sigma_h^3 \lambda_3 \omega_1 \omega_2 (\omega_1 - \omega_2) \frac{r'^2}{l^2} \right) dS_1\, dS_2. \tag{21}$$

The solution of the integral (21) is more easily achieved in a polar coordinates domain where through several algebraic manipulations (see Appendix A) we can finally find

$$I(\omega_1, \omega_2) = -2cR_p \frac{\pi^2 l^2}{k} \int_0^{\infty} e^{-j\tau_d(\omega_1 - \omega_2)}\, d\tau_d \tag{22}$$

where

$$\tau_d = \frac{r_1^2}{2cR_p}$$

and

$$k = a^2\sigma_h^2\omega_1\omega_2 + j\,\tfrac{2}{3}\,a^3\sigma_h^3\lambda_3\omega_1\omega_2(\omega_1-\omega_2). \quad (23)$$

Introducing this result in (20), we have

$$\langle E_s(\tau)E_s^*(\tau)\rangle = -\frac{R_p l^2\Gamma(\theta)\cos^2\theta}{2c(R_{10}R_{30})^2}\int_{-\infty}^{+\infty}\int_{-\infty}^{+\infty} \cdot\,\omega_1\omega_2 F(\omega_1)F^*(\omega_2)e^{-(1/2)a^2\sigma_h^2(\omega_1-\omega_2)^2} \cdot\frac{1}{k}\int_0^{\infty} e^{j(\tau-\tau_d)(\omega_1-\omega_2)}\,d\tau_d\,d\omega_1\,d\omega_2 \quad (24)$$

and assuming a Gaussian spectrum for the (compressed) radar pulse, we obtain

$$\langle E_s(\tau)E_s^*(\tau)\rangle = -\frac{R_p l^2\Gamma(\theta)\cos^2\theta}{2a^2\sigma_h^2 c(R_{10}R_{30})^2}\int_{-\infty}^{+\infty}\int_{-\infty}^{+\infty} \cdot\frac{e^{-\sigma^2(\omega_1-\omega_0)^2}e^{-\sigma^2(\omega_2-\omega_0)^2}}{1+j\,\frac{2}{3}\,a\sigma_h\lambda_3(\omega_1-\omega_2)}\cdot\frac{\sigma^2}{\pi}\cdot e^{-(1/2)a^2\sigma_h^2(\omega_1-\omega_2)^2} \cdot\int_0^{\infty} e^{j(\tau-\tau_d)(\omega_1-\omega_2)}\,d\tau_d\,d\omega_1\,d\omega_2. \quad (25)$$

As a further step to find a solution to the above integral, we can change the integration variables ω_1 and ω_2 into the variables $x=\omega_1-\omega_0$ and $y=\omega_2-\omega_0$

$$\langle E_s(\tau)E_s^*(\tau)\rangle = -\frac{R_p l^2\Gamma(\theta)\cos^2\theta}{2a^2\sigma_h^2 c(R_{10}R_{30})^2}\,\frac{\sigma^2}{\pi}\cdot\int_{-\infty}^{+\infty}\int_{-\infty}^{+\infty} \cdot\frac{e^{-\sigma^2(x^2+y^2)}}{\left[1+j\,\frac{2}{3}\,a\sigma_h\lambda_3(x-y)\right]}\,e^{-(1/2)a^2\sigma_h^2(x-y)^2} \cdot\int_0^{\infty} e^{j(\tau-\tau_d)(x-y)}\,d\tau_d\,dx\,dy. \quad (26)$$

Afterwards, letting $\gamma = x-y$, we can write

$$\langle E_s(\tau)E_s^*(\tau)\rangle = -\frac{R_p l^2\Gamma(\theta)\cos^2\theta}{2a^2\sigma_h^2 c(R_{10}R_{30})^2}\,\frac{\sigma^2}{\pi}\int_{-\infty}^{+\infty}\int_{-\infty}^{+\infty} \cdot\frac{e^{-\sigma^2\gamma^2}e^{-2\sigma^2 y(\gamma+y)}}{1+j\,\frac{2}{3}\,a\sigma_h\lambda_3\gamma}e^{-(1/2)a^2\sigma_h^2\gamma^2} \cdot\int_0^{\infty} e^{j(\tau-\tau_d)\gamma}\,d\tau_d\,d\gamma\,dy \quad (27)$$

and performing the integration over the variable y we obtain

$$\int_{-\infty}^{+\infty} e^{-2\sigma^2 y(\gamma+y)}\,dy = \sqrt{\frac{\pi}{2}}\,\frac{e^{\sigma^2\gamma^2/2}}{\sigma}. \quad (28)$$

Introducing (28) into (27), we have, after a few algebraic manipulations

$$\langle E_s(\tau)E_s^*(\tau)\rangle = -\frac{R_p l^2\Gamma(\theta)\sigma^2\cos^2\theta}{2\pi a^2\sigma_h^2 c\sigma(R_{10}R_{30})^2}\cdot\sqrt{\frac{\pi}{2}}\int_{-\infty}^{+\infty} \cdot\frac{e^{-(1/2)(\sigma^2+a^2\sigma_h^2)\gamma^2}}{\left[1+j\,\frac{2}{3}\,a\sigma_h\lambda_3\gamma\right]}\int_0^{\infty} e^{j(\tau-\tau_d)\gamma}\,d\tau_d\,d\gamma. \quad (29)$$

Performing the integration over the variable γ (see Appendix B) we obtain

$$\int_{-\infty}^{+\infty}\frac{e^{-(1/2)(\sigma^2+a^2\sigma_h^2)\gamma^2}e^{j(\tau-\tau_d)\gamma}}{1+j\,\frac{2}{3}\,a\sigma_h\lambda_3\gamma}\,d\gamma = \frac{3\pi}{a\sigma_h\lambda_3}\,e^{-(3/2a\sigma_h\lambda_3)(\tau-\tau_d-\tau_d')} \cdot\frac{1}{2}\left[1+\mathrm{Erf}\left(\frac{\tau-\tau_d-2\tau_d'}{\sqrt{2}\sqrt{\sigma^2+a^2\sigma_h^2}}\right)\right] \quad (30)$$

where

$$\tau_d' = \frac{3(\sigma^2+a^2\sigma_h^2)}{4a\sigma_h\lambda_3} \quad (31)$$

and the integral (29) becomes

$$\langle E_s(\tau)E_s^*(\tau)\rangle = \frac{3R_p l^2\Gamma(\theta)\sigma\cos^2\theta}{2a^3\sigma_h^3\lambda_3 c(R_{10}R_{30})^2}\sqrt{\frac{\pi}{2}} \cdot\int_0^{+\infty}\exp\left(-\frac{3}{2a\sigma_h\lambda_3}(\tau-\tau_d-\tau_d')\right) \cdot\frac{1}{2}\left[1+\mathrm{Erf}\left(\frac{\tau-\tau_d-2\tau_d'}{\sqrt{2}\sqrt{\sigma^2+a^2\sigma_h^2}}\right)\right]d\tau_d. \quad (32)$$

Finally, working out the integration over the variable τ_d, we obtain the following (see Appendix C):

$$\langle E_s(\tau)E_s^*(\tau)\rangle = \frac{R_p c l^2\Gamma(\theta)\sigma}{4\sigma_h^2(R_{10}R_{30})^2}\sqrt{\frac{\pi}{2}}\cdot\frac{1}{2} \cdot\left\{1+\mathrm{Erf}\left(\frac{\tau}{\sqrt{2}\sqrt{\sigma^2+a^2\sigma_h^2}}\right) -\exp\left(-\frac{3}{2a\sigma_h\lambda_3}(\tau-\tau_d')\right) \cdot\left[1+\mathrm{Erf}\left(\frac{\tau-2\tau_d'}{\sqrt{2}\sqrt{\sigma^2+a^2\sigma_h^2}}\right)\right]\right\}. \quad (33)$$

An approximated solution of the integral (29) is derived in Appendix D, resulting in the following more explicit expression of the skewness contribution to the average power echo time behavior:

$$\langle E_s(\tau)E_s^*(\tau)\rangle = \frac{R_p c l^2\Gamma(\theta)\sigma}{4\sigma_h^2(R_{10}R_{30})^2}\sqrt{\frac{\pi}{2}}\cdot\frac{1}{2} \cdot\left\{1+\mathrm{Erf}\left(\frac{\tau}{\sqrt{2}\sqrt{\sigma^2+a^2\sigma_h^2}}\right) -\frac{4}{3}\,\frac{a\sigma_h\lambda_3}{\sqrt{\sigma^2+a^2\sigma_h^2}}\,\frac{1}{\sqrt{2\pi}} \cdot\exp\left(-\frac{\tau^2}{2(\sigma^2+a^2\sigma_h^2)}\right)\right\}. \quad (34)$$

It is easily seen that the mean power echo in the non-Gaussian case is given by the sum of two contributions: the first term [given by (34) for $\lambda_3=0$] is the average power echo generated from a Gaussian surface, while the second

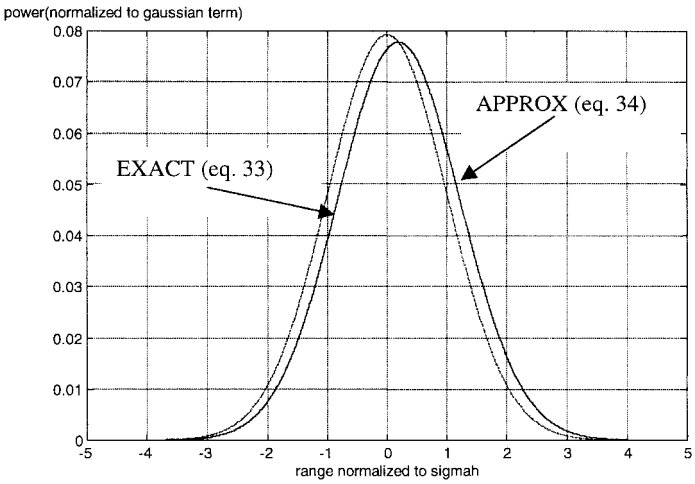

Fig. 3. Envelope of the skewness related term ($\sigma_h = 5$ m).

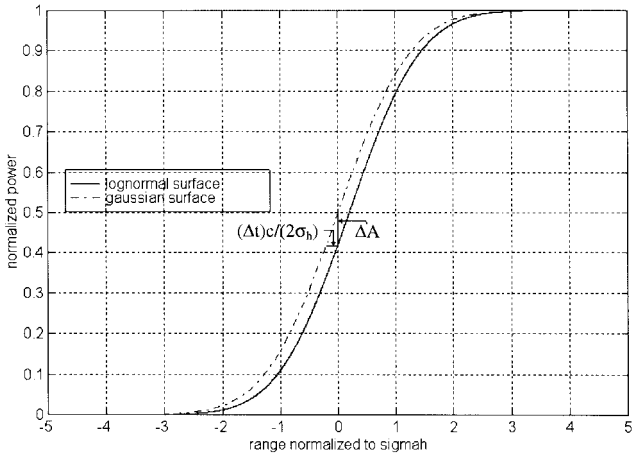

Fig. 4. Example of mean power echo for the lognormal surface case (SWH $= 20$ m, $\lambda_3 = 0.3$).

term takes into account for the presence of a skewness in the surface height distribution. It is worth noting that if $\lambda_3 = 0$ and $\theta = 0$ (that is we have a monostatic radar observing a Gaussian surface), we find

$$\langle E_s(\tau)E_s^*(\tau)\rangle = \frac{d^2\Gamma(0)\sigma}{4\sigma_h^2 R^3}\sqrt{\frac{\pi}{2}}\cdot\frac{1}{2} \cdot\left[1+\mathrm{Erf}\left(\frac{\tau}{\sqrt{2}\cdot\sqrt{\sigma^2+\left(\frac{2}{c}\sigma_h\right)^2}}\right)\right] \tag{35}$$

that is fully consistent with the well known Brown model [1].

The envelope of the skewness related term is shown in Fig. 3, while the overall power echo is plotted in Fig. 4 in the case of a high skewness coefficient and high sea roughness (the significant wave height is defined as SWH $= 4\sigma_h$). As easily seen the main effect of the skewness of the distribution is a small range delay, while the distortion is almost negligible.

The range delay induced by the skewness is given by[2]

$$\Delta r = \frac{c}{2}\Delta t = \frac{2}{3}\sigma_h\lambda_3\cos\theta. \tag{36}$$

In conclusion, it can be stated that the only relevant effect of the height skewness is the range offset expressed by (36), so that the mean power echo derived in (33) and (34) can be

[2]In order to evaluate the range delay induced by the skewness, we use the following approximation:

$$\mathrm{Erf}\left(\frac{t}{\sqrt{2}\sigma_{eq}}\right) = \frac{2}{\sqrt{2\pi}\sigma_{eq}}e^{-(t^2/2\sigma_{eq}^2)}\Big|_{t=0}t+\cdots\approx\frac{2t}{\sqrt{2\pi}\sigma_{eq}}.$$

Considering now (35), we observe that the skewness-related term causes a shift of a quantity ΔA on the Gaussian echo, thus leading to a corresponding time shift expressed by $\Delta t = (\sqrt{2\pi}\sigma_{eq}/2)\Delta A$ where we used the approximation of constant slope near $t = 0$ due to the small values of the expected time shift. The value of ΔA can be approximated by the skewness term evaluated in $t = 0$; that is $\Delta A = (4/3)(a\sigma_h\lambda_3/\sigma_{eq})(1/\sqrt{2\pi})$. From the latter and Δt we immediately obtain (36).

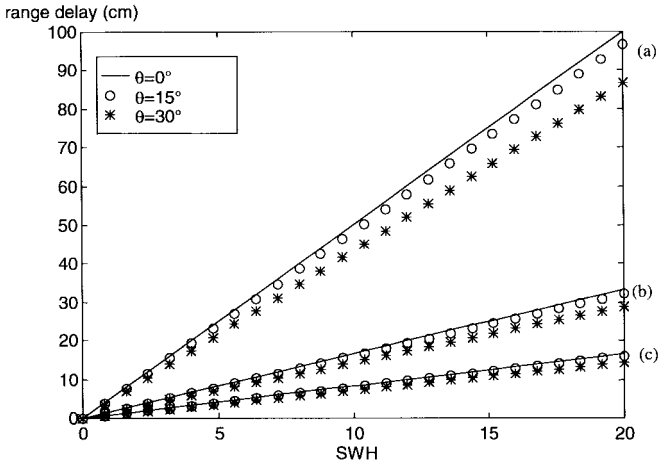

Fig. 5. Range delay versus SWH: (a) $\lambda_3 = 0.3$. (b) $\lambda_3 = 0.1$. (c) $\lambda_3 = 0.05$.

approximated by the following expression:

$$\langle E_s(\tau)E_s^*(\tau)\rangle = \frac{R_p d^2\Gamma(\theta)\sigma}{4\sigma_h^2(R_{10}R_{30})^2}\sqrt{\frac{\pi}{2}}\cdot\frac{1}{2} \cdot\left[1+\mathrm{Erf}\left(\frac{\tau-\frac{2}{c}\Delta r}{\sqrt{2}\sqrt{\sigma^2+a^2\sigma_h^2}}\right)\right] \tag{37}$$

where Δr is given by (36), and is plotted versus SWH in Fig. 5 for different values of the incidence angle (θ) and skewness coefficient (λ_3).

The range offset Δr quoted above is known as electromagnetic (EM) bias, because it causes a constant error in the range measurement. As clear from (36), such error shows a linear dependence on the surface roughness and skewness coefficient and is inversely proportional to the incidence angle through the cosine dependence. Hence, the maximum delay is obtained in the monostatic altimetry case, i.e., when $\theta = 0$. This behavior could have been predicted based on the physical nature of such error; in fact, usual estimators estimate the range delay of the returned echo, fitting the received echoes to the echo

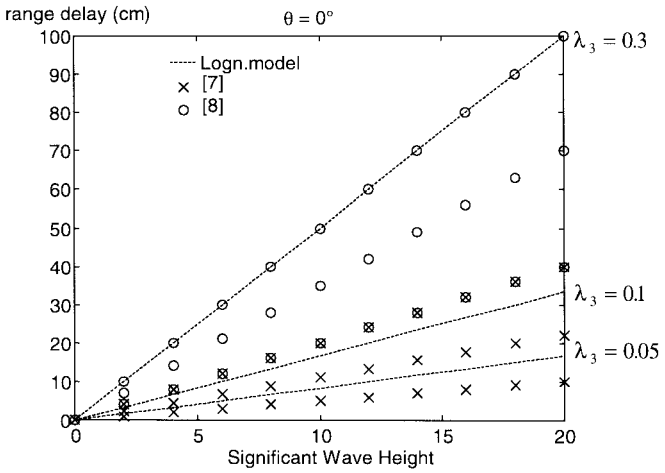

Fig. 6. Experimental determination of EM bias with regard to analytical model.

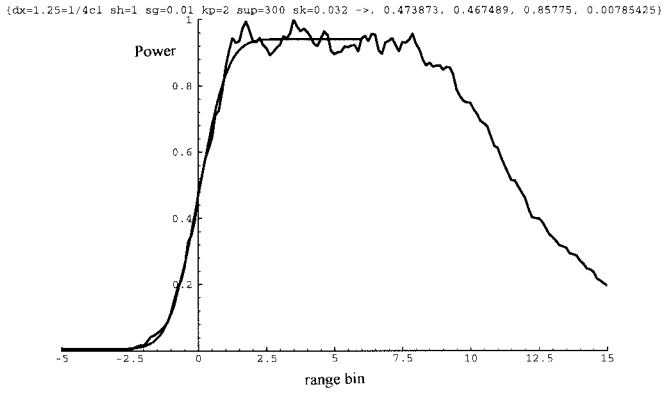

Fig. 7. Example of nonlinear fit between the simulated echo and the analytical model. The four numbers above the curves on the right are, respectively, the parameters A, B, C, and x_0 of the model. The numbers on the left are the input parameters to the simulator.

model obtained by considering only the Gaussian term in (33) and (34), i.e., assuming $\lambda_3 = 0$ [in the monostatic case this echo model is the well known Brown model presented in [1] and in (35)]. This turns into tracking the median surface, which is certainly different from the mean surface in presence of a nonzero skewness λ_3, thus introducing a bias in the measurement. Moreover, it is straightforward to note that this gap between the median and mean values is directly related to the asymmetry factor (i.e., the skewness coefficient) and to the sea state (i.e., the rms height). The inverse dependence on the incidence angle can be explained with the fact that the radar actually senses the rms height projected on the slant range direction, which is actually given by $\sigma_h \cos\theta$.

Experimental determinations of EM bias have been undertaken by using a nadir-looking radar altimeter carried on an aircraft at 36 GHz [7] and at 10 GHz [8]; the results of these determinations are also reported in [4] and can be summarized as follows.

- It has been found that an EM bias of about -1.1% of SWH has a scatter between -0.5 and -2.0% [7];
- It has been found that an EM bias of about -3.5% of SWH has a scatter between -2.0 and -5.0% [8].

The behaviors of the corresponding biases against the SWH are plotted in Fig. 6 along with the theoretical values computed by means of (36).

III. Simulation

In order to check the effectiveness of the simplifications used in the analytic evaluation of the electromagnetic bias [(36) and Fig. 5] and to assess the feasibility of the achieved model a numeric simulation of the mean power echo scattered from an irregular surface has been performed. The scattered electric field has been computed by directly solving the integral (1) as a coherent sum of the contributions arising from a very large number of facets that approximate the observed surface according to the Kirchhoff theory. In order to ensure a sufficient accuracy in the surface representation, the actual surface has been sampled so that four samples at least are taken per surface correlation length. The size and orientation of the single facet with respect to the radar line of sight have been evaluated according to the height of two adjacent samples along two orthogonal reference directions. Finally, each facet has been considered like a small antenna reradiating according to the specific geometry [15].

The simulation has been performed in a scaled scenario (the altitude of the radar sensor is 2000 m and the size of the observed region is 400×400 m^2) in order to reduce the computational burden due to the very large number of facets needed to model the surface and in the monostatic case since only in this case we have from the literature some experimental results that can be used as a reference to test the simulation program.

In order to extract the information on the electromagnetic bias, the simulated echo waveform averaged over 150 independent observations is processed by performing a best fitting with the function $A + B \cdot \mathrm{Erf}[C(x - x_0)]$ and the resulting x_0 is assumed as output value of the electromagnetic bias Δr. As an example the result of a simulation is shown in Fig. 7: the averaged output waveform is plotted superimposed to the above mentioned reference function with the A, B, C, and x_0 parameters computed according to a nonlinear fit algorithm.

Running several simulations values of Δr has been obtained for different values of the sea rms height and of the skewness coefficient. These values are plotted in Fig. 8 as dots, along with the theoretical behavior found in the previous section (36) as a function of the surface parameter σ_g [which is roughly one third of the skewness coefficient as from (14)] and for a sea surface rms height of 1 or 2 m.

As it can be seen from the above mentioned figure, there is a fairly good agreement between analytic and simulation results, so that the developed model can be effectively used in the performance assessment of a bistatic altimeter operating on a skewed surface. This could have been predicted to some extent since the various approximations introduced affect mainly the angular behavior of the bistatic scattering coefficient, which acts on the shape of the tail of the average echo waveform. On the other hand, the measurement of the range delay and, thus, the EM bias extent, strongly relies on the leading edge of such waveform, which is primarily driven by the behavior of the bistatic scattering coefficient at near specular reflection angles.

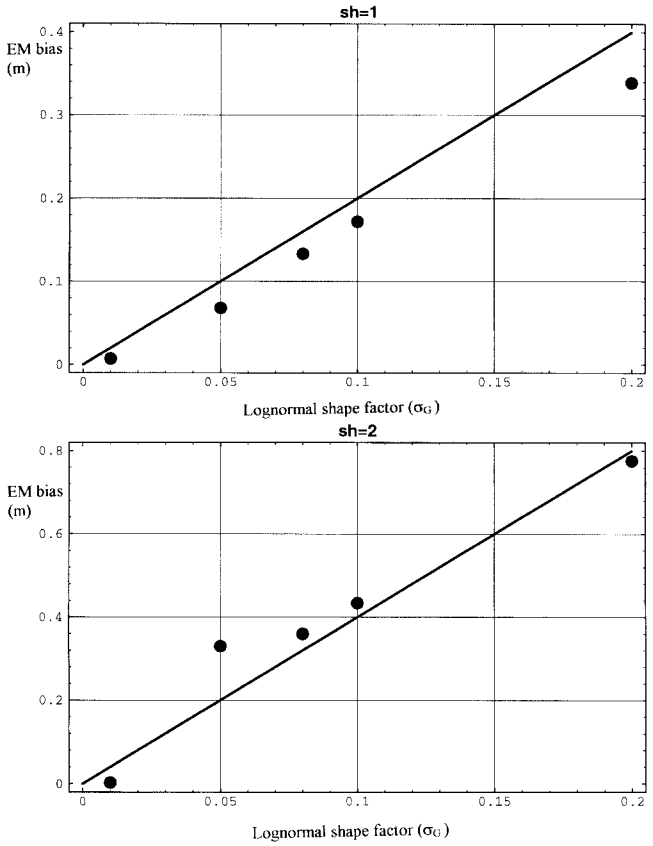

Fig. 8. Comparison between EM bias analytical model (solid line) and its evaluation obtained by simulation.

IV. Conclusions

We have derived a model of the average received echo of a bistatic altimeter for ocean observation. The model has been evaluated applying the Kirchhoff approximation to write the integral of the scattered electric field and solving this integral under the hypothesis of non-Gaussian random rough surface with Gaussian correlation.

The result is an average echo behaving roughly like an error function, but incorporating also a time shift which depends on the surface roughness and skewness (electromagnetic bias). An explicit closed-form expression for such EM bias has been presented and its effectiveness was demonstrated by numerical simulations.

Moreover, the power of the scattered field shows a $\cos^3(\theta)$ behavior [see (37) and the geometry depicted in Fig. 1], which is in full agreement with the result obtained by writing the radar equation for a rough surface. In fact, in this case the radar cross section is given by $\sigma^0 A$ and it can be easily demonstrated that the area A depends on $(\cos^2\theta)^{-1}$ [16] while the backscattering coefficient as discussed in [3] and [6] can be written as $\sigma^0 = \gamma \cos\theta$ where γ is a constant depending on the surface dielectric characteristics. This result has been also checked by numerical simulations [5].

As demonstrated in this paper, applying the bistatic model to the case of nadir-looking altimeter and Gaussian surface, we obtain a result which is fully consistent with the Brown model, whereas considering the case of nadir-looking altimeter and non-Gaussian surface, we have found electromagnetic bias values very close to those reported by various authors in literature. Hence, the model presented in the paper can be considered useful to implement optimum (or suboptimum) estimators of the surface parameters, based, in general, on model fitting techniques. In this regard, first preliminary evaluations of the theoretical Rao–Cramer bounds for the estimation errors have confirmed that (as well known) the electromagnetic bias cannot be estimated and removed from the received echo with classical maximum likelihood approach. Moreover, regarding the height measurement accuracy, for SWH in the range 1–20 m and 1000 integrated pulses, a range delay accuracy below about 5 cm, practically independent of the incidence angle, can be accomplished.

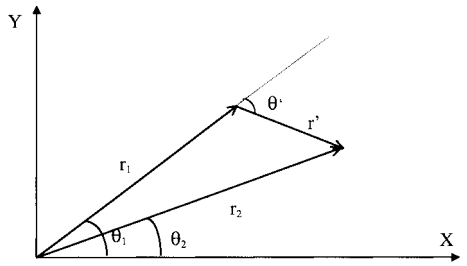

Fig. 9. Definition of the new variables for the solution of the integral (A.1).

Appendix A

In order to solve (21), it is convenient to rewrite it in the following form (polar coordinates, see also Fig. 9):

$$I(\omega_1,\omega_2)=\int_0^{\infty}\int_0^{2\pi}\int_0^{\infty}\int_0^{2\pi} \cdot\exp\left(-j\,\frac{1}{2cR_p}\left[\omega_1 r_1^2-\omega_2 r_2^2\right]\right) \cdot\exp\left(-k\,\frac{r'^2}{l^2}\right) r_1 r_2\,dr_1\,d\theta_1\,dr_2\,d\theta_2 \quad \text{(A.1)}$$

where

$$k=a^2\sigma_h^2\omega_1\omega_2+j\,\tfrac{2}{3}a^3\sigma_h^3\lambda_3\omega_1\omega_2(\omega_1-\omega_2). \quad \text{(A.2)}$$

This integral can be simplified by changing the integration variables r_2, θ_2 into r' and θ', according to the geometry depicted in Fig. 9.

The following Jacobian must be evaluated to perform the coordinates transformation

$$J(r',\theta')=\begin{vmatrix}\dfrac{\partial r_2}{\partial r'} & \dfrac{\partial r_2}{\partial \theta'}\\[2ex] \dfrac{\partial \theta_2}{\partial r'} & \dfrac{\partial \theta_2}{\partial \theta'}\end{vmatrix}. \quad \text{(A.3)}$$

Considering that

$$\begin{aligned} r'\,\mathrm{sen}\,\theta' &= r_2\,\mathrm{sen}(\theta_1-\theta_2)\\ r_2\cos(\theta_1-\theta_2) &= r_1+r'\cos\theta' \end{aligned} \quad \text{(A.4)}$$

we can write

$$\theta_2 = \theta_1 - \operatorname{artg}\left(\frac{r' \operatorname{sen}\theta'}{r_1 + r' \cos\theta'}\right)$$
$$r_2 = \sqrt{r_1^2 + r'^2 + 2r'r_1 \cos\theta'} \tag{A.5}$$

$$\frac{\partial r_2}{\partial r'} = \frac{r' + r_1 \cos\theta'}{\sqrt{r_1^2 + r'^2 + 2r'r_1 \cos\theta'}}$$
$$\frac{\partial r_2}{\partial \theta'} = -\frac{r'r_1 \operatorname{sen}\theta'}{\sqrt{r_1^2 + r'^2 + 2r'r_1 \cos\theta'}} \tag{A.6}$$

$$\frac{\partial \theta_2}{\partial r'} = -\frac{1}{1 + \left(\dfrac{r' \operatorname{sen}\theta'}{r_1 + r' \cos\theta'}\right)^2} \cdot \left(\frac{\operatorname{sen}\theta'}{r_1 + r' \cos\theta'} - \frac{r' \operatorname{sen}\theta' \cdot \cos\theta'}{(r_1 + r' \cos\theta')^2}\right)$$
$$= -\frac{1}{1 + \left(\dfrac{r' \operatorname{sen}\theta'}{r_1 + r' \cos\theta'}\right)^2} \frac{r_1 \operatorname{sen}\theta'}{(r_1 + r' \cos\theta')^2}$$
$$= -\frac{r_1 \operatorname{sen}\theta'}{(r_1 + r' \cos\theta')^2 + (r' \operatorname{sen}\theta')^2}$$
$$= -\frac{r_1 \operatorname{sen}\theta}{r_1^2 + r'^2 + 2r'r_1 \cos\theta'} \tag{A.7}$$

$$\frac{\partial \theta_2}{\partial \theta'} = -\frac{1}{1 + \left(\dfrac{r' \operatorname{sen}\theta'}{r_1 + r' \cos\theta'}\right)^2} \cdot \left(\frac{r' \cos\theta'}{r_1 + r' \cos\theta'} + \frac{r'^2 \operatorname{sen}^2\theta'}{(r_1 + r' \cos\theta')^2}\right)$$
$$= -\frac{1}{1 + \left(\dfrac{r' \operatorname{sen}\theta'}{r_1 + r' \cos\theta'}\right)^2} \cdot \frac{r'r_1 \cos\theta' + r'^2}{(r_1 + r' \cos\theta')^2}$$
$$= -\frac{r'r_1 \cos\theta' + r'^2}{(r_1 + r' \cos\theta')^2 + (r' \operatorname{sen}\theta')^2}. \tag{A.8}$$

Then

$$J(r', \theta') = \frac{r' + r_1 \cos\theta'}{\sqrt{r_1^2 + r'^2 + 2r'r_1 \cos\theta'}} \cdot \left(-\frac{r'r_1 \cos\theta' + r'^2}{(r_1 + r' \cos\theta')^2 + (r' \operatorname{sen}\theta')^2}\right) - \left(-\frac{r_1 \operatorname{sen}\theta}{r_1^2 + r'^2 + 2r'r_1 \cos\theta'}\right) \cdot \left(-\frac{r'r_1 \operatorname{sen}\theta'}{\sqrt{r_1^2 + r'^2 + 2r'r_1 \cos\theta'}}\right)$$
$$= \frac{(-r'^3 - r_1 r'^2 \cos\theta' - r_1^2 r' \cos^2\theta' - r_1 r'^2 \operatorname{sen}^2\theta')}{(r_1^2 + r'^2 + 2r'r_1 \cos\theta)^{3/2}}$$
$$= -\frac{r'}{\sqrt{r_1^2 + r'^2 + 2r'r_1 \cos\theta}}$$
$$= -\frac{r'}{r_2}. \tag{A.9}$$

Then (23) becomes

$$I = \int_0^\infty r_1 \cdot r' \cdot dr_1 \cdot \int_0^{2\pi} d\theta_1 \cdot \int_0^\infty J(r', \theta') \cdot dr' \cdot \int_0^{2\pi} d\theta' \cdot \exp\left(-j \frac{1}{2cR_p}(\omega_1 r_1^2 - \omega_2 r_1^2)\right) \cdot \exp\left(-j \frac{\omega_2}{2cR_p}(r'^2 + 22r'r_1 \cos\theta')\right) \exp\left(-k \frac{r'^2}{l^2}\right)$$
$$= -2cR_p\pi \int_0^\infty \exp\left(-j \frac{r_1^2}{2cR_p}(\omega_1 - \omega_2)\right) \cdot \frac{dr_1^2}{2cR_p} \cdot \int_0^\infty \int_0^{2\pi} \exp\left(-j \frac{\omega_2}{2cR_p}(r'^2 + 2r'r_1 \cos\theta')\right) \cdot \exp\left(-k \frac{r'^2}{l^2}\right) r' \cdot dr' \cdot d\theta'. \tag{A.10}$$

In order to obtain an approximated expression of the integral (A.10), we can analyze the two exponential terms in the last double integral $\int_0^\infty \int_0^{2\pi} e^{-j(\omega_2/2cR_p)(r'^2 + 2r'r_1 \cos\theta')} \cdot e^{-k(r'^2/l^2)} r' \cdot dr' \cdot d\theta'$ and observe that the exponential term $e^{-k(r'^2/l^2)}$ is the one that dominates the behavior of the integral. As a matter of fact if we evaluate, in a typical operating geometry, the two terms of the first exponential, we can find

- first term $\rightarrow \dfrac{\omega r'^2}{2cR_p} = \dfrac{\pi r'^2}{\lambda R_p} = \dfrac{\pi \cdot 36 \cdot 10^{-4}}{8 \cdot 10^5 \cdot 0.0214}$
$$\cong 7 \cdot 10^{-7}\text{rad}$$
- second term $\rightarrow \dfrac{2\pi \cdot 2r'r_1}{2R_p\lambda} = \dfrac{2\pi}{R_p\lambda} \cdot 0.06 \cdot \dfrac{\lambda R_p}{2L}$
$$\cong 0.2\text{rad}$$

where we have evaluated $r' = l/\sqrt{k} = l\lambda/4\pi\sigma_h \cos\vartheta = \lambda\sqrt{2}/4\pi m \cos\vartheta \cong 0.06 \cdot \text{m}$ approximating $\omega_1 \cdot \omega_2 \cong \omega_0^2$ and giving to the rms surface slope $m = \sqrt{2} \cdot \sigma_h/l$ a typical lower value (0.04), in order to make reference to a worst case. For the same reason we have let r_1 equal to the radius of the antenna beam footprint, by considering a typical antenna diameter of 1 m.

In this worst case we have

$$\int_0^\infty \int_0^{2\pi} \exp\left(-j \frac{\omega_2}{2cR_p}(r'^2 + 2r'r_1 \cos\theta')\right) \cdot \exp\left(-k \frac{r^2}{l^2}\right) r' \cdot dr' \cdot d\theta'$$
$$\cong \int_0^\infty \int_0^{2\pi} \exp(-j(0.2)) \exp\left(-k \frac{r^2}{l^2}\right) r'\, dr'\, d\theta'$$
$$\cong \int_0^\infty \int_0^{2\pi} \exp\left(-k \frac{r'^2}{l^2}\right) r'\, dr'\, d\theta' \tag{A.11}$$

and then we can conclude that this approximation can be reasonably considered valid in conventional operating conditions. As a consequence the integral (A.8) can be simplified and rewritten in the form of (22).

APPENDIX B

We need to solve the following integral in γ [see (29)]

$$I = \int_{-\infty}^{+\infty} \frac{e^{-(1/2)(\sigma^2+a^2\sigma_h^2)\gamma^2}}{1+j\,\frac{2}{3}a\sigma_h\lambda_3\gamma}\, e^{j(\tau-\tau_d)\gamma}\, d\gamma. \tag{B.1}$$

This expression can be rewritten in a more compact form making the following assumptions:

$$\begin{aligned} I &= \int_{-\infty}^{+\infty} \frac{e^{-\alpha\gamma^2}}{1+jc\gamma}\, e^{j\gamma t}\, d\gamma \\ \alpha &= \tfrac{1}{2}(\sigma^2+a^2\sigma_h^2) \\ t &= \tau-\tau_d \\ c &= \tfrac{2}{3}a\sigma_h\lambda_3. \end{aligned} \tag{B.2}$$

Letting $\gamma = 2\pi f$ (A.2) becomes

$$I = 2\pi \int_{-\infty}^{+\infty} \frac{e^{-2\pi^2 2\alpha f^2}}{1+j2\pi fc}\, e^{j2\pi ft}\, df \tag{B.3}$$

which can be thought of as the inverse Fourier transform of the product of the following two functions:

$$\begin{aligned} F_1(f) &= e^{-2\pi^2 2\alpha f^2} \\ F_2(f) &= \frac{1}{1+j2\pi fc}. \end{aligned} \tag{B.4}$$

Applying the convolution theorem to (B.3) we can write

$$\begin{aligned} I &= 2\pi \int_{-\infty}^{+\infty} F_1(f)F_2(f)e^{j2\pi ft}\, df \\ &= 2\pi \int_{-\infty}^{+\infty} f_1(\tau)f_2(t-\tau)\, d\tau \end{aligned} \tag{B.5}$$

being $f_1(t)$ and $f_2(t)$ the inverse Fourier transforms of $F_1(f)$ and $F_2(f)$. Taking the inverse Fourier transforms of (B.4) we obtain

$$\begin{aligned} f_1(t) &= \frac{1}{\sqrt{2\pi}\sqrt{2\alpha}}\, e^{-(t^2/4\alpha)} \\ f_2(t) &= \frac{1}{c}\, e^{-(t/c)}u_{-1}(t) \end{aligned} \tag{B.6}$$

and introducing (B.6) in (B.5) yields

$$\begin{aligned} I &= 2\pi \int_{-\infty}^{+\infty} \frac{1}{\sqrt{2\pi}\sqrt{2\alpha}}\, \exp\left(-\frac{\tau^2}{4\alpha}\right)\frac{1}{c} \\ &\quad \cdot \exp\left(-\frac{(t-\tau)}{c}\right)u_{-1}(t-\tau)\, d\tau \\ &= \sqrt{\frac{\pi}{\alpha}}\,\frac{1}{c}\, \exp\left(-\frac{t}{c}\right)\int_{-\infty}^{t} \exp\left(-\frac{\tau^2}{4\alpha}+\frac{\tau}{c}\right)d\tau \\ &= \sqrt{\frac{\pi}{\alpha}}\,\frac{1}{c}\, \exp\left(-\frac{t}{c}+\frac{\alpha}{c^2}\right)\int_{-\infty}^{t} \exp\left(-\left(\frac{\tau-2\alpha/c}{2\sqrt{\alpha}}\right)^2\right)d\tau \\ &= \sqrt{\frac{\pi}{\alpha}}\,\frac{1}{c}\, \exp\left(-\frac{t}{c}+\frac{\alpha}{c^2}\right)\sqrt{\pi} \\ &\quad \cdot \int_{-\infty}^{1/2\sqrt{\alpha}(t-(2\alpha/c))} \frac{1}{\sqrt{\pi}}\, \exp\left(-y^2\right)2\sqrt{\alpha}\, dy \\ &= \frac{2\pi}{c}\, \exp\left(-\frac{1}{c}\Big(t-\frac{\alpha}{c}\Big)\right)\cdot\frac{1}{2}\left\{1+\mathrm{Erf}\left(\frac{t-\dfrac{2\alpha}{c}}{2\sqrt{\alpha}}\right)\right\} \end{aligned} \tag{B.7}$$

where the Error function is defined by

$$\mathrm{Erf}\{t\} = \frac{2}{\sqrt{\pi}}\int_0^t e^{-y^2}\, dy. \tag{B.8}$$

Substituting the parameters defined in (B.2) into (B.7) we obtain

$$\begin{aligned} I = \frac{3\pi}{a\sigma_h\lambda_3}\, &\exp\left(-\frac{3}{2a\sigma_h\lambda_3}\,(t-\tau_d-\tau_d')\right)\cdot\frac{1}{2} \\ &\cdot\left\{1+\mathrm{Erf}\left(\frac{t-\tau_d-2\tau_d'}{\sqrt{2}\sqrt{\sigma^2+a^2\sigma_h^2}}\right)\right\} \end{aligned} \tag{B.9}$$

where

$$\tau_d' = \frac{3(\sigma^2+a^2\sigma_h^2)}{4a\sigma_h\lambda_3}.$$

that is (30).

APPENDIX C

Recalling (32) we have to perform the following integration in the variable τ_d

$$\begin{aligned} I' = \int_0^{+\infty} &\exp\left(-\frac{3}{2a\sigma_h\lambda_3}\,(\tau-\tau_d-\tau_d')\right)\frac{1}{2} \\ &\cdot\left\{1+\mathrm{Erf}\left(\frac{\tau-\tau_d-2\tau_d'}{\sqrt{2}\sqrt{\sigma^2+a^2\sigma_h^2}}\right)\right\}d\tau_d. \end{aligned} \tag{C.1}$$

Integrating by parts yields

$$\begin{aligned} I' &= \frac{1}{\alpha}\,\exp(-\alpha(\tau-\tau_d-\tau_d'))\cdot\frac{1}{2} \\ &\quad\cdot\left\{1+\mathrm{Erf}\left(\frac{\tau-\tau_d-2\tau_d'}{\sqrt{2}\sigma_{eq}}\right)\Bigg|_{\tau_d=0}^{\infty}\right\} \\ &\quad-\frac{1}{\alpha}\,\frac{1}{\sqrt{2\pi}\sigma_{eq}}\int_0^{+\infty}\exp(-\alpha(\tau-\tau_d-\tau_d')) \\ &\quad\cdot\exp\left(-\frac{(\tau-\tau_d-2\tau_d')^2}{2\sigma_{eq}^2}\right)d\tau_d \\ &= -\frac{1}{\alpha}\Bigg[\exp(-\alpha(\tau-\tau_d'))\,\frac{1}{2} \\ &\qquad\cdot\left\{1+\mathrm{Erf}\left(\frac{\tau-2\tau_d'}{\sqrt{2}\sigma_{eq}}\right)\right\}-\frac{1}{\sqrt{2\pi}\sigma_{eq}}\cdot\int_0^{+\infty} \\ &\qquad\cdot\exp\left(-\alpha(\tau-\tau_d-\tau_d')-\frac{(\tau-\tau_d-2\tau_d')^2}{2\sigma_{eq}^2}\right)d\tau_d\Bigg] \end{aligned} \tag{C.2}$$

where

$$\begin{aligned} \alpha &= \frac{3}{2a\sigma_h\lambda_3} \\ \sigma_{eq} &= \sqrt{\sigma^2+a^2\sigma_h^2}. \end{aligned} \tag{C.3}$$

Now we change the variable τ_d into $\theta = (\tau - \tau_d - 2\tau_d')/(\sqrt{2}\sigma_{eq})$, thus having from (C.2)

$$\begin{aligned} I' = &-\frac{1}{\alpha}\left[\exp(-\alpha(\tau-\tau_d'))\,\frac{1}{2}\cdot\left\{1+\mathrm{Erf}\left(\frac{\tau-2\tau_d'}{\sqrt{2}\sigma_{eq}}\right)\right\}\right. \\ &\quad -\frac{1}{\sqrt{\pi}}\exp\left(-\alpha\tau_d'+\frac{\alpha^2}{2}\sigma_{eq}^2\right)\cdot\int_{-\infty}^{(\tau-2\tau_d')/\sqrt{2}\sigma_{eq}} \\ &\left.\cdot\exp\left(-\left(\theta+\frac{\alpha\sigma_{eq}}{\sqrt{2}}\right)^2\right)d\vartheta\right] \\ = &-\frac{1}{\alpha}\left[\exp(-\alpha(\tau-\tau_d'))\,\frac{1}{2}\left\{1+\mathrm{Erf}\left\{\frac{\tau-2\tau_d'}{\sqrt{2}\sigma_{eq}}\right\}\right\}\right. \\ &\quad -\frac{1}{\sqrt{\pi}}\exp\left(-\alpha\tau_d'+\frac{\alpha^2}{2}\sigma_{eq}^2\right) \\ &\left.\cdot\int_{-\infty}^{((\tau-2\tau_d')/\sqrt{2}\sigma_{eq})+(\alpha\sigma_{eq}/\sqrt{2})}\exp(-y^2)\,dy\right] \\ = &-\frac{1}{\alpha}\left[\exp(-\alpha(\tau-\tau_d'))\cdot\frac{1}{2}\left\{1+\mathrm{Erf}\left(\frac{\tau-2\tau_d'}{\sqrt{2}\sigma_{eq}}\right)\right\}\right. \\ &-\exp\left(-\alpha\tau_d'+\frac{\alpha^2}{2}\sigma_{eq}\right)\cdot\frac{1}{2} \\ &\left.\cdot\left\{1+\mathrm{Erf}\left(\frac{\tau-2\tau_d'+\alpha\sigma_{eq}^2}{\sqrt{2}\sigma_{eq}}\right)\right\}\right. \end{aligned} \tag{C.4}$$

Substituting the parameter α and recalling the definition of τ_d' given in (31), we finally obtain

$$\begin{aligned} I' = &\frac{2a\sigma_h\lambda_3}{3}\left[\frac{1}{2}\left\{1+\mathrm{Erf}\left(\frac{\tau}{\sqrt{2}\sigma_{eq}}\right)\right\}\right. \\ &-\exp\left(-\frac{3}{2a\sigma_h\lambda_3}(\tau-\tau_d')\right)\frac{1}{2} \\ &\left.\cdot\left\{1+\mathrm{Erf}\left(\frac{\tau-2\tau_d'}{\sqrt{2}\sigma_{eq}}\right)\right\}\right]. \end{aligned} \tag{C.5}$$

Substituting (C.5) in (32) leads to the final expression of the mean power echo, given by (33).

Appendix D

Recalling again (29) we want to find a solution of the following integral in γ

$$I = \int_{-\infty}^{+\infty}\frac{e^{-(1/2)(\sigma^2+a^2\sigma_h^2)\gamma^2}}{1+j\,\frac{2}{3}a\sigma_h\lambda_3\gamma}\,e^{j(\tau-\tau_d)\gamma}\,d\gamma \tag{D.1}$$

different from the one described in Appendix B.

As a matter of fact, the integral (D.1) can also be interpreted as the output signal from a single-pole low pass filter when the input signal has a Gaussian behavior. Such a filter can be expressed also in terms of the corresponding single pole high-pass filter. Thus the integral (D.1) can be rewritten as

$$\begin{aligned} I = &\int_{-\infty}^{+\infty}\exp\left(-\tfrac{1}{2}(\sigma^2+a^2\sigma_h^2)\gamma^2\right) \\ &\cdot\left[1-\frac{j\,\frac{2}{3}a\sigma_h\lambda_3\gamma}{1+j\,\frac{2}{3}a\sigma_h\lambda_3\gamma}\right]\exp(j(\tau-\tau_d)\gamma)\,d\gamma. \end{aligned} \tag{D.2}$$

The cutoff frequency of the high-pass filter is

$$\omega_0 = \frac{3}{2a\sigma_h\lambda_3} \tag{D.3}$$

while the bandwidth of the input signal can be assumed to be

$$\sigma_f = \frac{1}{\sqrt{\sigma^2+a^2\sigma_h^2}} \cong \frac{1}{a\sigma_h}. \tag{D.4}$$

For typical values of λ_3, we have that $\omega_0 > \sigma_f$ and we can approximate the transfer function of the high pass filter with a straight line, meaning that the output signal is a scaled version of the time derivative of the input signal. Under this assumption we can rewrite (D.2) in the following form:

$$\begin{aligned} I = &\int_{-\infty}^{+\infty}\exp\left(-\tfrac{1}{2}(\sigma^2+a^2\sigma_h^2)\gamma^2\right) \\ &\cdot\left[1-j\,\tfrac{2}{3}a\sigma_h\lambda_3\gamma\right]\exp(j(\tau-\tau_d)\gamma)\,d\gamma \\ = &I_1+I_2. \end{aligned} \tag{D.5}$$

Resolving first I_1, we have

$$\begin{aligned} I_1 &= \int_{-\infty}^{+\infty}\exp\left(-\frac{1}{2}(\sigma^2+a^2\sigma_h^2)\gamma^2\right)\exp(j(\tau-\tau_d)\gamma)\,d\gamma \\ &= \frac{\sqrt{2\pi}}{\sqrt{\sigma^2+a^2\sigma_h^2}}\exp\left(-\frac{(\tau-\tau_d)^2}{2(\sigma^2+a^2\sigma_h^2)}\right). \end{aligned} \tag{D.6}$$

Resolving for I_2 we have

$$\begin{aligned} I_2 = &-\tfrac{2}{3}a\sigma_h\lambda_3\int_{-\infty}^{+\infty}j\gamma\exp\left(-\tfrac{1}{2}(\sigma^2+a^2\sigma_h^2)\gamma^2\right) \\ &\cdot\exp(j(\tau-\tau_d)\gamma)\,d\gamma \\ = &-\frac{2}{3}a\sigma_h\lambda_3 2\pi\frac{d}{dt} \\ &\cdot\left[\frac{1}{\sqrt{2\pi}\sqrt{\sigma^2+a^2\sigma_h^2}}\exp\left(-\frac{t^2}{2(\sigma^2+a^2\sigma_h^2)}\right)\right]_{t=\tau-\tau_d} \\ = &\frac{2}{3}a\sigma_h\lambda_3\sqrt{2\pi}\,\frac{\tau-\tau_d}{(\sigma^2+a^2\sigma_h^2)^{3/2}}\exp\left(-\frac{(\tau-\tau_d)^2}{2(\sigma^2+a^2\sigma_h^2)}\right). \end{aligned} \tag{D.7}$$

Substituting (D.6) and (D.7) in (D.5) we obtain

$$\begin{aligned} I = &\frac{\sqrt{2\pi}}{\sqrt{\sigma^2+a^2\sigma_h^2}}\exp\left(-\frac{(\tau-\tau_d)^2}{2(\sigma^2+a^2\sigma_h^2)}\right) \\ &+\frac{\sqrt{2\pi}(\tau-\tau_d)}{(\sigma^2+a^2\sigma_h^2)^{3/2}}\,\frac{2}{3}a\sigma_h\lambda_3\exp\left(-\frac{(\tau-\tau_d)^2}{2(\sigma^2+a^2\sigma_h^2)}\right). \end{aligned} \tag{D.8}$$

To compute the average power echo given by (29), we need then to solve the following integral in τ_d:

$$I' = \int_0^{+\infty} I(\tau,\tau_d)\,d\tau_d = I_1'(\tau)+I_2'(\tau). \tag{D.9}$$

Considering only the first contribution, we have

$$\begin{aligned} I_1'(\tau) &= \int_0^{\infty}\frac{\sqrt{2\pi}}{\sqrt{\sigma^2+a^2\sigma_h^2}}\exp\left(-\frac{(\tau-\tau_d)^2}{2(\sigma^2+a^2\sigma_h^2)}\right)d\tau_d \\ &= -\frac{\sqrt{2\pi}}{\sqrt{\sigma^2+a^2\sigma_h^2}}\int_{-\infty}^{\tau}\exp\left(-\frac{\theta^2}{2(\sigma^2+a^2\sigma_h^2)}\right)d\theta \\ &= 2\pi\cdot\frac{1}{2}\cdot\left\{1+\mathrm{Erf}\left[\frac{\tau}{\sqrt{2}\sqrt{\sigma^2+a^2\sigma_h^2}}\right]\right\}. \end{aligned} \tag{D.10}$$

Integrating the second contribution, we have

$$I_2'(\tau) = \sqrt{2\pi}\,\frac{2}{3}\,\frac{a\sigma_h\lambda_3}{\sqrt{\sigma^2+a^2\sigma_h^2}}\int_0^\infty \frac{(\tau-\tau_d)}{\sigma^2+a^2\sigma_h^2} \cdot \exp\left(-\frac{(\tau-\tau_d)^2}{2(\sigma^2+a^2\sigma_h^2)}\right)d\tau_d$$
$$= -\sqrt{2\pi}\,\frac{2}{3}\,\frac{a\sigma_h\lambda_3}{\sqrt{\sigma^2+a^2\sigma_h^2}} \cdot \exp\left(-\frac{\tau^2}{2(\sigma^2+a^2\sigma_h^2)}\right). \quad \text{(D.11)}$$

Introducing (D.10) and (D.11) in (D.9), we obtain

$$I'(\tau) = 2\pi\left\{\frac{1}{2}\left\{1+\mathrm{Erf}\left[\frac{\tau}{\sqrt{2}\sigma_{eq}}\right]\right\} - \frac{2}{3}\,\frac{a\sigma_h\lambda_3}{\sqrt{\sigma^2+a^2\sigma_h^2}}\,\frac{1}{\sqrt{2\pi}}\,\exp\left(-\frac{\tau^2}{2\sigma_{eq}^2}\right)\right\} \quad \text{(D.12)}$$

that is (34).

REFERENCES

[1] G. S. Brown, "The average impulse response of a rough surface and its applications," *IEEE Trans. Antennas Propagat.*, vol. AP-25, pp. 67–74, Jan. 1977.

[2] M. Martin-Neira, "A passive reflectometry and interferometry system (PARIS): Application to ocean altimetry," *ESA J.*, vol. 17, pp. 331–355, 1993.

[3] N. J. Willis, *Bistatic Radar*. Norwood, MA: Artech House, 1991.

[4] A. K. Fung and H. J. Eom, "Coherent scattering of a spherical wave from an irregular surface," *IEEE Trans. Antennas Propagat.*, vol. AP-31, pp. 68–72, Jan. 1983.

[5] A. Ciaffone, G. Picardi, and R. Seu, "Application of the Paris concept to the GPS signals," Studi Tecnologie Sistemi, Rome, Italy, Tech. Rep. TR-1-3/1/95, ESA Contract 142286-27/06/94.

[6] F. T. Ulaby, A. K. Fung, and R. K. Moore, *Microwave Remote Sensing—Active and Passive*. Reading, MA: Addison-Wesley, 1988, vol. II.

[7] E. Rodriguez, "Altimetry for non-Gaussian oceans: Height biases and estimation of parameters," *J. Geophys. Res.*, vol. 93, pp. 14.107–14.120, Nov. 1988.

[8] B. Levine, *Fondaments Theoriques de la Radiotechnique Statistique*. Moscow, Russia: MIR, 1984.

[9] "Topography observing system study," Studi Tecnologie Sistemi, Rome, Italy, Tech. Rep. TR/STS/001/97, Alenia Spazio Contract TLR/ALS/AR/19/96.

[10] D. E. Barrick and B. J. Lipa, "Analysis and interpretation of altimeter sea echo," *Adv. Geophys.*, vol. 27, pp. 60–99, 1985.

[11] M. A. Srokosz, "On the joint distribution of surface elevation and slopes for a non linear random sea, with application to radar altimetry," *J. Geophysical Research*, vol. 91, pp. 995–1005, Jan. 1986.

[12] L. Imperi and M. Ugolini, "The lognormal distribution," INFO-COM Dept., University of Rome "La Sapienza," Rome, Italy, Tech. Rep. TR002/5/97, Feb. 1997.

[13] E. J. Walsh, D. W. Hancock, and D. E. Hines, "Electromagnetic bias of 36-GHz radar altimeter measurement of MSL," *J. Marine Geodesy*, vol. 8, pp. 265–296, 1984.

[14] L. W. Choy, D. L. Hammond, and E. A. Uliana, "Electromagnetic bias of 10 GHz radar altimeter measurement of MSL," *J. Marine Geodesy*, vol. 8, pp. 296–312, 1984.

[15] S. Alessi, F. De Acutis, G. Picardi, and R. Seu, "Surface bistatic scattering coefficient by means of the facet model," in *Proc. 26th Eur. Microwave Conf.*, Prague, Czech Republic, Sept. 1996, pp. 337–340.

[16] "Requirements and concepts for topography observing system," TOS Study Team, Alemia Aerospaco, Rome, Italy, final presentation to ESA/ESTEC, Mar. 1997.

[17] A. K. Fung and H. J. Eom, "Multiple scattering and depolarization by a randomly rough Kirchhoff surface," *IEEE Trans. Antennas Propagat.*, vol. AP-29, pp. 463–471, May 1981.

Giovanni Picardi received the Laurea degree in electrical engineering from the University of Rome "La Sapienza," Rome, Italy, in 1960.

In 1961, he joined the Research and Development Laboratory of Selenia S.p.A., Rome, Italy, where he worked on radar signal processing matters. In 1970 he joined the University of Perugia, Italy, where he taught cybernetics and information theory. In 1975 he joined the University of Bari, Bari, Italy, as Full Professor of electrical communications. Since 1978 he has been with the INFO-COM Department, University of Rome "La Sapienza" as a Professor of remote sensing systems. He has been involved in several projects for the European Space Agency (ESA) and the Italian Space Agency (ASI). He has been a member of the Science Team for the definition of the ROSETTA mission, the mission MORO (Moon Orbiting Observatory), and the mission INTERMARSNET. He is currently a member of the Cassini Radar Science Team and Co-Investigator of the experiment CONSERT of the mission Rosetta. Recently, he has been appointed Principal Investigator (PI) of the subsurface sounding radar altimeter experiment, a cooperation between University of Rome and the Jet Propulsion Laboratory, Pasadena, CA, which has been selected to fly on the ESA Mars Express mission launching in 2003. He is the author of more than 130 publications (including conferences) concerning radar signal processing, and system analysis. His main interest is in radar design for civil and military applications and remote sensing (e.g., SAR-X and ERS-1).

Roberto Seu received the Laurea degree in electronic engineering and the Ph.D. degree in information and communication theory from the University of Rome "La Sapienza," Rome, Italy.

In 1986, he joined Contraves Italiana S.p.A. as a Radar System Engineer. In 1992, he joined the INFO-COM Department, University of Rome "La Sapienza" after winning a national competitive examination as Research Fellow. He has participated in a feasibility study of a multimode radar system in the frame of the mission MORO and is currently a member of the Cassini Radar Science Team and Co-Investigator of the experiment Consert of the mission Rosetta, where he is also responsible of the complete development of the bread board of the analog subsystem. He is also a Co-Investigator in the Mars Express subsurface sounding radar altimeter (SSRA) experiment. His main interest is in active remote sensing.

Stefano G. Sorge was born in Naples, Italy, in 1973. He received the Laurea degree in telecommunications engineering (*cum laude*) from the University of Rome "La Sapienza," Rome, Italy, in 1996.

In 1997, he served as an Italian Air Force Officer. Since 1997 he has been engaged at the INFO-COM Department of the University of Rome "La Sapienza," involved in system analysis and algorithm design for active remote sensing instruments. He is currently a Co-Investigator in the subsurface sounding radar altimeter (SSRA) experiment, which has been recently selected to fly on the ESA Mars Express mission in 2003. His main research interests are in the field of statistical scattering modeling, high-resolution imaging, radar interferometry, and subsurface probing techniques.

Manuel Martin Neira received the M.S. and Ph.D. degrees in telecommunication engineering from the School of Telecommunication Engineering of the Polytechnic University of Catalonia, Spain, in 1986 and 1996, respectively.

In 1988, he work on radiometry at ESTEC (European Space Research and Technology Center) under a a fellowship. From 1989 to 1992 he joined Grupo Mecanica de Vuelo (GMV), a Spanish firm, where he was responsible for several projects for the European Space Agency (ESA) related to Global Positioning System (GPS) spacecraft navigation with application to precise landing and attitude determination. Since 1992 (with ESA), he has worked in the Payload Systems Division of ESTEC, in charge of technology development for radiometer systems and providing support to the definition of the European Global Navigation Satellite System 2 (GNSS-2). He is responsible for the study on three carrier ambiguity resolution that should allow real-time very precise relative positioning in GNSS-2. He has authored or coauthored more than 50 papers on navigation, earth observation using navigation signals, and microwave radiometry.

Mr. Neira is a member of the Working Group on Ambiguity Resolution for the International Association of Geodesy.